Available online at www.sciencedirect.com
SCIENCE DIRECT®
International Journal of Heat and Mass Transfer 47 (2004) 1079–1089
International Journal of HEAT and MASS TRANSFER
www.elsevier.com/locate/ijhmt

Modelling and numerical simulation of convection driven high pressure induced phase changes

W. Kowalczyk *, Chr. Hartmann, A. Delgado

Lehrstuhl für Fluidmechanik und Prozessautomation, TU München, Weihenstephaner Steig 23, D-85350 Freising, Germany

Received 17 January 2003; received in revised form 23 June 2003

Abstract

High pressure induced freezing and thawing processes are investigated by means of modelling and numerical simulation. The enthalpy–porosity model is reformulated in terms of conservation equations of mass, momentum and heat for a compressible medium. It can be shown that convective fluid motion has a major influence on the formation of the ice front. Furthermore, due to a vanishing density anomaly under high pressure, natural convection exhibits a different behaviour than under low pressure thus the formation of the ice front under high pressure obeys different mechanisms than that under ambient pressure.

Keywords: Phase change; Heat transfer; Natural convection

1. Introduction

The treatment of food and biotechnological substances with high hydrostatic pressures (HHP) up to 1 GPa is generally carried out at ambient temperature in a batch process, where the substance is compressed to the desired pressure level maintained throughout several minutes. High hydrostatic pressure has manifold effects such as phase transitions, the denaturation of proteins, the inactivation of enzymes or the inactivation of microorganisms while aroma compounds and vitamins are preserved. Consequently, a wide spectrum of potential applications in food technology is related to high pressure effects. Besides a pasteurizing effect of high pressure treatment, sensorial properties, functional properties and shelf life are affected [1–3]. This is often related to the unfolding of proteins and modifications of the activities of enzymes during the HHP treatment [4].

Pressure induced freezing/thawing has the advantage that the cellular structure of food remains intact in this process due to smaller crystal size of the contained ice leading to reduced damage of the texture of plant and animal tissues, smaller risk of microbial infection and less cellular drip [5–7]. Moreover, the latent heat which is released during a thermally driven freezing process is smaller under high pressure and represents a potentially smaller demand of resources.

The phase diagram of water in the range between atmospheric pressure and 500 MPa is shown in Fig. 1. From this diagram it can be seen, that water, or food containing mainly water, can be cooled without phase change below 273 K. Thus, the freezing and thawing can be controlled through an additional parameter—pressure. Ice 'I' as solid phase can be obtained at maximum pressure of 207.5 MPa and a minimum temperature of 252 K. Additionally, the density of ice 'I' is lower than the density of water. For other types of ice, the density is larger than the density of water and the melting temperature always increases with the pressure.

There are different kinds of high pressure freezing and thawing processes. Fig. 1 shows two of them: high pressure shift freezing/thawing (HPSF/T) and high pressure assisted freezing/thawing (HPAF/T). In high pressure shift freezing and thawing processes the phase transition occurs only due to active decompression. In

* Corresponding author. Tel.: +49-81-61-71-4003; fax: +49-81-61-71-4510.
E-mail address: kowalczyk@wzw.tum.de (W. Kowalczyk).

0017-9310/$ - see front matter © 2003 Elsevier Ltd. All rights reserved.
doi:10.1016/j.ijheatmasstransfer.2003.07.030

Nomenclature

H	total enthalpy
$\vec{V}$	velocity vector
ΔH	enthalpy of solidification
c	specific heat
C_1	Darcy constant
C_2	computational constant
f	volume fraction
g	gravity
K	porosity function
L	latent heat
p	pressure
S	source term
T	temperature
t	time

Greek symbols

ρ	density
η	viscosity

Subscripts

l	liquid
liq	liquidus
num	numeric form of source term
sol	solidus
s	solid
0	initial value

Superscripts

n	value at the previous iteration of the current time step
$n+1$	value at the current iteration of the current time step
0	value of the converged solution from the previous time step

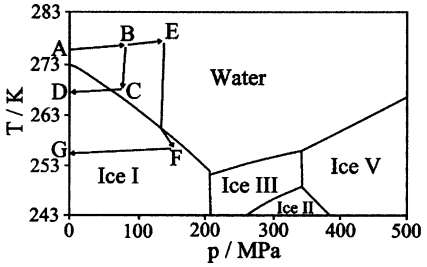

Fig. 1. Phase diagram of water. ABCD/DCBA—high pressure shift freezing/thawing; ABEFG/GFEBA—high pressure assisted freezing/thawing.

order to induce phase transition during HP-assisted processes the temperature is decreased below melting temperature at almost constant elevated pressures.

Since phase changes are driven by both pressure and temperature, heat transfer effects play a major role in this field. The time scales of cooling and heating under high pressure have to be respected with great care in order to achieve a complete phase transition in every location of the high pressure chamber. Especially, when packed substances are frozen or thawed, the interaction between the heat transfer within the packed food, across the packaging material and in the pressure medium becomes complex. This effect is further influenced by the pressure dependency of the physical properties of the involved substances and by convective motion of the liquid volume fraction. The pressure dependency of the physical properties of water is known [8–10] up to a certain extent but shows to be weaker than for e.g. edible oils, where for example the viscosity increases over several orders of magnitude under high pressure [10].

The pressure increase is achieved by compression and, in the case of water, is generally accompanied by a temperature increase of around 2–3 K per 100 MPa, which leads to a spatial and temporal distribution of the temperature and of the fluid velocity as observed by Pehl and Delgado [11] and Pehl et al. [12] using experimental techniques and by Hartmann [13] using numerical simulation. The effect of convective transport on the pressure induced biotechnological conversion is investigated by Hartmann and Delgado [14,15] who show that thermal heterogeneities combined with convective transport strongly affects the spatial homogeneity of the inactivation of an enzyme or of micro-organisms.

Since the experimental investigation of field distributions of temperature, phase change processes and fluid velocity in a near industrial scale is always accompanied by difficulties related to the equipment and the requirement of optical accessibility, modelling and simulation in connection with local experimental information obtained from thermocouple-measurements seems to be a more efficient choice, especially when a scale up analysis is required.

Up to now, in the modelling of phase changes under high hydrostatic pressure only heat conduction phenomena have been considered [16,17]. Since modelling of phase changes at high pressure accounting for fluid motion is not trivial, many efforts have been made to provide experimental data, where convection is suppressed. In order to avoid fluid motion in an phase changes experiment, pure water and 4.3% NaCl aqueous solution was used in a high porosity matrix (foam with

0.98 porosity) by Chourot et al. [18]. The other way to prevent convection is to use a substance which transforms into a gel with increasing pressure.

In the present paper, the HHP freezing and thawing process will be assessed taking into account convective effects, since in the above mentioned contributions convective transport has been shown to be of significant influence on the homogeneity of the HHP process. Following subjects are going to be addressed:

- A model accounting for both conductive and convective heat, momentum and mass transfer has to be derived and validated with experimental data for the ambient pressure case and the high pressure case.
- An analysis of convective fluid motion in proximity of the phase limit is delivered for pure water and compared to the ambient pressure case for a small scale laboratory high pressure chamber.
- The influence of convective fluid motion on the formation of the ice front is going to be investigated for this configuration as well as for a medium size laboratory high pressure device.

In this context several contributions on modelling and simulation of the solidification problems for water, aqueous solutions and for metallic melts accounting for fluid motion at ambient pressure are taken into consideration. Giangi et al. [19] present the numerical investigation of natural convection during ice formation and compare the results with own experiments. They analyse the influence of boundary conditions, mesh dependence and 3D effects on the freezing process at ambient pressure. The experimental results will serve as validation data in the present contribution.

The conservation equations for systems with phase change have been derived for a continuum formulation by Bennon and Incropera [23] as well as Ni and Incropera [20]. These equations are reformulated in the present paper in order to account for compressibility. The numerical solution technique introduced by Brent and Voller [21], Voller and Prakash [22] or Bennon and Incropera [23], Voller et al. [24] are adopted and enhanced for the case of compressible media under high hydrostatic pressure.

2. Governing equations

In order to derive the governing equations for the considered process, the authors follow the ideas of [23,24], where a conservation law for a solid–liquid phase change system in a continuum formulation is derived from the combination of an infinitive number of components and phases including physically motivated assumptions about interactions between the different phases and components. These equations are reformulated for the case of compressible media and are described in a concise manner subsequently. An ample description of the equations and their limitations can be found in [23]. The equation system in the present paper contains the equation of mass conservation

$$\frac{\partial \rho}{\partial t} + \nabla \cdot (\rho \vec{V}) = 0, \tag{1}$$

the equation of energy conservation

$$\frac{\partial}{\partial t}(\rho H) + \nabla \cdot (\rho \vec{V} H) = \frac{\partial p}{\partial t} + \nabla \cdot (k \nabla T) - \frac{\partial}{\partial t}(\rho f_l \Delta H) - \nabla \cdot (\rho f_l \vec{V}_l \Delta H). \tag{2}$$

In order to account for the balance of the enthalpy of solidification ΔH two sink terms are integrated in the equation containing additionally the liquid volume fraction f_l and the velocity of the liquid $\vec{V}_l$. The velocity $\vec{V}$ equals $f_l \vec{V}_l$ since $\vec{V} = f_l \vec{V}_l + f_s \vec{V}_s$ and $\vec{V}_s \equiv \vec{0}$ according to the form introduced by Voller et al. [24].

The liquid volume fraction is defined as

$$f_l = \begin{cases} 1, & \text{if } T > T_{liq}, \\ \dfrac{H - H_{sol}}{H_{liq} - H_{sol}}, & \text{if } T_{sol} < T < T_{liq}, \\ 0, & \text{if } T < T_{sol}. \end{cases} \tag{3}$$

The pure substances, e.g. pure water solidifies without a mushy region. Nevertheless, for phase changes of pure water the temperature difference between T_{liq} and T_{sol} is introduced for numerical convenience and amounts up to 0.5 K. Since the aim of the investigation is to provide a model for the simulation of phase changes in aqueous solutions and real food with substantial differences between T_{liq} and T_{sol}, this is supposed to be an admissible simplification.

The enthalpy of solidification is calculated from

$$\Delta H = \int (c_l - c_s)\, \mathrm{d}T + L. \tag{4}$$

The equation of momentum conservation can be written as

$$\rho \left[\frac{\partial \vec{V}}{\partial t} + (\vec{V} \cdot \nabla)\vec{V} \right] = -\nabla p + \nabla \cdot \left(\eta_l \frac{\rho}{\rho_l} \nabla \vec{V} \right) - \frac{\eta_l}{K} \frac{\rho}{\rho_l} (\vec{V} - \vec{V}_s). \tag{5}$$

This equation has a sink term, too, which governs the momentum transfer on the interface between the liquid and the solid phase and is called the Carman–Kozeny porosity model, e.g. Brent et al. [21]. It becomes active in the solid region and in the mushy region, where both liquid and solid phases are coexistent. At the beginning of solidification, this term generates a viscous stress, which decelerates the fluid in the mushy region and

enforces zero velocity in the solid region. The Carman–Kozeny porosity model is described by permeability coefficient K, which form is

$$K = C_1 \cdot \left(\frac{f_l^3}{(1-f_l)^2 + C_2} \right), \tag{6}$$

where C_1 is the Darcy constant known from experiments and C_2 is a constant, which has no physical significance. C_2 is chosen in the order of magnitude of 10^{-3} to avoid a division by zero. For example for the mushy region of water and ice the values of 1.6×10^4 and 1.6×10^9 are used for C_1 and compared in [25]. There are small differences in the velocity field and in shape of ice in the results of both cases. From the experiences of the authors of the present contribution the value 1.6×10^5 can be recommended, since it engenders fastest convergence. It is supposed that the permeability parameter C_1 can also depend on the pressure since high pressure induced changes in the mushy region have to be expected. However, this possibility is not taken into account at present. The high pressure processing influences the cellular structure of food. The numerical model described in this paper takes into account only macroscopic effects. Changes in the micro-structure will manifest integrally in the modified thermo-physical properties of the considered food.

It is assumed that the flow in the HP-chamber is laminar. In accordance to Bennon and Incoprera [23] the columnar dendritic structure is supposed to be valid in the mushy region and the velocity of the solid phase is equal to zero. Supercooling and nucleation phenomena are not taken into account at present.

3. Numerical methods

The governing equations are solved with the finite volume method using a commercial software framework CFX-4.4 (ANSYS CFX) enhanced by own subroutines covering about 6000 lines of FORTRAN 90 statements.

The equation of state of water and ice is taken from the contribution of Nagornov and Chizhov [9]. The specific heat capacity is calculated by using the relationship from the work of Saul and Wagner [8]. The density of water can also be calculated with this equation of state but the time of the computation is much longer due to the more complicated form of equation than the equation of Nagornov and Chizhov. The viscosity of water is taken from [10]. The implementation of the Carman–Kozeny porosity model is straightforward and can be carried out by adding Eq. (6) as a body force to the conservation equation of momentum.

The implementation of the source terms in the conservation equation of energy needs further numerical treatment in order to assure diagonal dominance of the resulting system of algebraic equations. The source term

$$S = -\frac{\partial}{\partial t}(\rho f_l \Delta H) - \nabla \cdot (\rho f_l \vec{V}_l \Delta H) \tag{7}$$

is dependent on the total enthalpy H via the liquid volume fraction and ΔH. From Eq. (4) it can be seen that the enthalpy of solidification ΔH contains the latent heat L and an integral of difference between heat capacities of liquid and solid phases in the range between the liquidus and the solidus temperature. In some cases the integral quantity can be neglected. For pure substances, it can be assumed that the crystallisation process occurs isotherm. In this case the integral equals zero. If the heat capacities of both phases are equal, then the integral is zero as well. In the third case, the value from integral in comparison to latent heat can take small values. For example the heat capacity for water at 273 K is equal to about 4200 $\mathrm{J\,kg^{-1}\,K^{-1}}$ and for ice it is equal to 2260 $\mathrm{J\,kg^{-1}\,K^{-1}}$. Further, when the solidification occurs within a small temperature difference, e.g. 1°, the integral yields a value of 1940 $\mathrm{J\,kg^{-1}}$. The latent heat during the transition from liquid to solid is about 333,000 $\mathrm{J\,kg^{-1}}$ at ambient pressure and about 240,000 $\mathrm{J\,kg^{-1}}$ at 200 MPa. This estimate shows that the value from integral is two orders of magnitude smaller than the value of latent heat and has a negligible influence on the process. Supercooling will significantly increase the integral quantity due to a larger range between liquidus and solidus temperatures. With above presented considerations Eq. (7) can be discretised to

$$S_{\mathrm{num}} = -L\left[\frac{1}{\Delta t}\left(\rho^{n+1} f_l^{n+1} - \rho^0 f_l^0\right) + \nabla \cdot (\rho f_l \vec{V}_l)^{n+1}\right], \tag{8}$$

where the superscript $n+1$ denotes values at the current iteration of the current time step and subscript 0 denotes values of the converged solution from the previous time step. Since $\rho^{n+1} f_l^{n+1}$ depends on the conservation quantity H^{n+1}, the product at the present iteration has to be expressed as a function of H. This is done by the Taylor series expansion

$$\begin{aligned}\rho^{n+1} f_l^{n+1} &= \rho^n f_l^n + \left.\frac{\partial(\rho f_l)}{\partial H}\right|_{H^n} (H^{n+1} - H^n) \\ &= \rho^n f_l^n + \left(f_l^n \left.\frac{\partial \rho}{\partial H}\right|_{H^n} + \rho^n \left.\frac{\partial f_l}{\partial H}\right|_{H^n} \right)(H^{n+1} - H^n).\end{aligned} \tag{9}$$

Insertion of Eq. (9) in Eq. (8) followed by some mathematical transformations the source term yields

$$\begin{aligned}S_{\mathrm{num}} = -L\Bigg[\frac{1}{\Delta t}\Bigg(&\rho^n f_l^n - \rho^0 f_l^0 + \left(f_l^n \frac{\partial \rho^n}{\partial H^n} + \rho^n \frac{\partial f_l^n}{\partial H^n} \right) H^{n+1} \\ &- \left(f_l^n \frac{\partial \rho^n}{\partial H^n} + \rho^n \frac{\partial f_l^n}{\partial H^n} \right) H^n \Bigg) + \nabla \cdot (\rho f_l \vec{V}_l)^{n+1} \Bigg]\end{aligned} \tag{10}$$

allowing an integration into the main code as prescribed by the provider of CFX-4.4. The partial derivatives with respect to the total enthalpy can be obtained numerically from the equation of state and from Eq. (3). For cases in which phase transition occurs simultaneously with a pressure change the value of latent heat in the given equations must be taken into account as a variable leading to a more complicated structure of the numerical procedure.

4. Results

4.1. Simulation of convection during ice formation at ambient pressure

The first validation case for the numerical model is carried out for the phase change at ambient pressure, since experimental investigations of field distributions are available, which is not the case for the high hydrostatic pressure regime. The results are obtained using the current computational model and are compared with experimental and numerical results presented in [19]. The geometry of the computational domain is shown in Fig. 2. For the simulations only the quadratic cross-section with an edge length of 38 mm in the central z-plane of the hexahedral vessel is taken. A uniform mesh with 152×152 grid points and a time step of 0.2 s is used to solve the system of equations. On the vertical walls of the vessel the temperatures T_1 and T_2 are applied and on the horizontal walls a constant heat flux is prescribed. The thermal conditions and material properties of the walls to calculate a value of heat flux are described in [19].

Before the freezing process is started, steady state free convection in the vessel is generated by a prescribed temperature difference on the vertical walls ($T_1 = 283$ K and $T_2 = 273$ K). After about 3000 s, fluid motion and temperature distribution are in steady state. Fig. 3 presents the velocity field obtained with particle image velocimetry [19] (left) and with numerical simulation (right) which are in very good agreement. Also the temperature distribution (not shown) obtained from the numerical simulation is almost identical to the experimentally obtained field. Because of abnormal behaviour of water in the investigated range of temperature (density of water is maximum at 277 K), there are two main vortices separated at the isotherm line of 277 K.

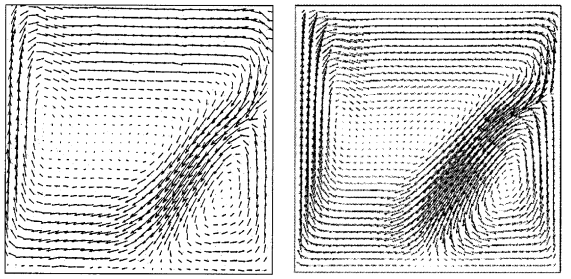

Fig. 3. Free steady state convection, experiment (left), numerical simulation (right).

The numerical results obtained after calculation of steady state free convection are applied as initial conditions for the freezing process. The freezing is provoked by a decrease in the temperature T_2 from 273 to 263 K during 120 s. Fig. 4 shows the observed flow structure and ice front during freezing after 2600 s in the central x-, y-plane for both experiment (left from [19]) and numerical simulation (right).

The part of the computational domain that is not covered by velocity vectors represents the solid phase. The shape and the position of the ice front as well as velocity distribution are in excellent agreement with the experimental results. Also the temperature fields of both experimental (not shown) and numerical data agree very well. The small differences in the shape of the ice front and in the temperature distribution [19] can be a consequence of the assumption that the heat flux on horizontal walls is constant; but in fact, the heat flux may be transient and variable along the walls.

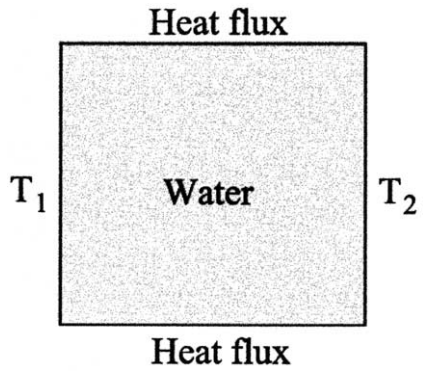

Fig. 2. Geometry of the computational domain.

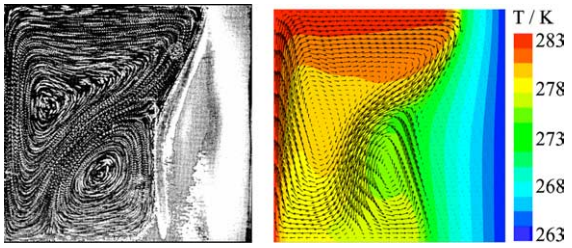

Fig. 4. Distribution of velocity, ice front and temperature in experiment (left from [19]) and numerical simulation (right) after 2600 s.

4.2. Validation with the data from the experiments with HP-equipment

In order to further validate the computational model, numerical simulations of solidification at ambient pressure and under HHP conditions are carried out and compared to the experimental results. The measurements have been carried out at the Institute of Food Biotechnology and Food Process Engineering (TU Berlin). The HP-unit (Unipress, Poland) used for the experiments has a maximal inner volume of 3.4 ml and is immersed in a temper bath with constant temperature during the complete process duration (see Fig. 5 up). The pressure is measured in the experiment with a manometer installed on the inlet tube of the pressure medium. The range of the manometer goes from ambient pressure to 1000 MPa. Moreover, a control unit holds the pressure on a constant level during the process. The chamber is optically not accessible making optical measurement systems for field distributions un-applicable. The information obtained from the experiments is temperature time characteristics at a central location within the chamber denominated as control point. At ambient and high pressure conditions, the temperature measurement is limited to one location due to the design of the experimental apparatus.

The dimensions of the chamber volume are specific for each of the two investigated cases. For the phase changes at ambient pressure the height is 37 mm and for the high pressure processes 22 mm. The diameter equals 9.8 mm. During ice formation the pressure has to be controlled by volume adaptation in order to keep it on a constant level since the specific volume of ice in region I is greater than that of water.

Taking advantage of the axis-symmetry of the chamber, a 2D cross-section (Fig. 5 down) with 185×25 grid points is used as computational domain. Time dependent boundary conditions are applied which are obtained from temperature profiles measured at the walls of the chamber. In order to achieve a stable convergent solution the time step is inferior to 0.2 s.

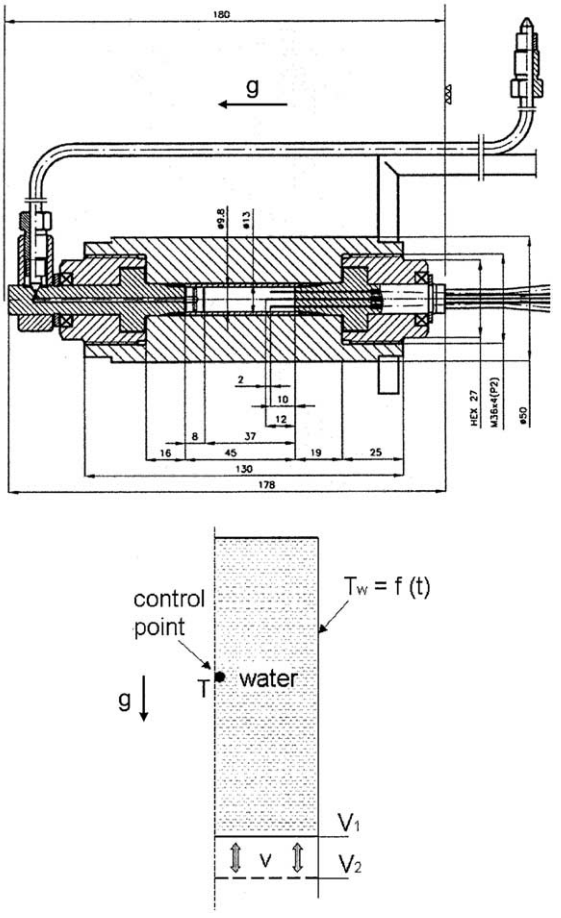

Fig. 5. Geometry of the high pressure chamber (up) and computational domain (down).

4.2.1. Phase change at ambient pressure

Water at a temperature of 293 K is poured in the HP-chamber at ambient pressure with the same initial temperature. After 1 min of thermal compensation the HP-chamber is immersed in a thermal control bath, which previously is cooled down to 253 K. In Fig. 6 the temperature time characteristics of the control point (in the centre of the sample) is shown for both experiment and simulation. Due to the cooling below the solidification limit the water is freezing from the walls to the centre of the chamber. It takes about 3 min to reduce the temperature in the centre from the initial value to the solidification temperature of 273 K. Supercooling can be observed in the experiment after 2.5 min indicated by the increase of the temperature due to a sudden release of the solidification enthalpy. A constant temperature level is observed for approximately 2 min during the following solidification. After the termination of the solidification, a further decrease of the temperature exists. After 10 min it is almost equal to the temperature of the

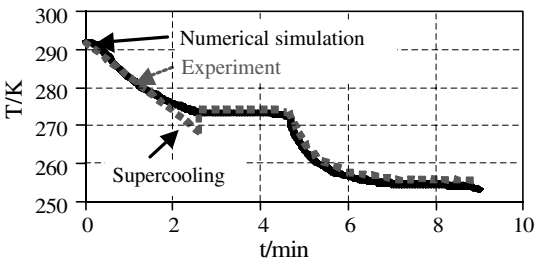

Fig. 6. Phase change at 0.1 MPa—experimental and numerical results.

cooling medium in the thermal control bath. For this case it can be concluded, that the numerical prediction agrees excellently with the experimental result. The location of the largest deviation can be observed at the moment when supercooling appears, which is not accounted for in the numerical model.

The temperature and velocity distribution is shown at 80 s after the immersion in the thermal control bath in Fig. 7a and at 120 s in Fig. 7b. The liquid volume fraction at 120 s is shown in Fig. 7c.

In Fig. 7a, the major part of the volume is at a temperature above 273 K, thus liquid. Solidification can be observed in a narrow region on the walls of the chamber. The density anomaly of water leads to the existence of two counter-rotating vortices. After 120 s the complete liquid volume is cooled below the critical temperature for the density anomaly of 277 K. Consequently, the flow pattern has changed and only one vortex persists rotating in counter-clockwise direction. A zone with temperatures above 276 K is concentrated in the upper centre resulting from fluid motion and convective heat transfer. The solid volume fraction shown in Fig. 7c is of almost constant thickness on the walls. Now influence of convective transport can be observed in this case. The longest vectors in Fig. 7 indicate velocity magnitudes of 0.6 mm s^{-1}.

4.2.2. Phase change at high hydrostatic pressure

The phase transition of water under HHP conditions at 100 MPa is presented subsequently as a further validation example. The temperature of the HP-chamber filled with water has a constant value of 283 K at the beginning. The water is pressurized up to 100 MPa during 13.5 s and simultaneously its average temperature increases for 2 K. After 2 min of pressure holding the HP-unit is immersed into the thermal control bath having a temperature of 243 K. The temperature at the

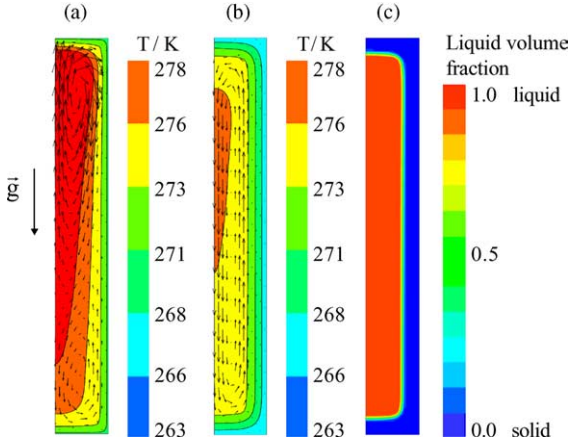

Fig. 7. The temperature and the liquid volume fraction distribution during freezing at 0.1 MPa.

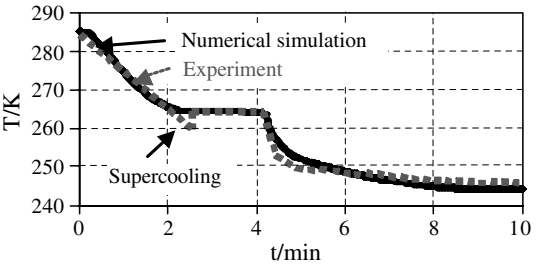

Fig. 8. Phase change at 100 MPa—experimental and numerical results.

control point in the centre of the chamber is monitored in Fig. 8 for both experimental and numerical results. The formation of ice on the walls at 260 K releasing latent heat causes the persistance of a constant temperature level at 264 K after 2.5 min of cooling. The phase change propagates to the centre and is achieved after slightly more than 4 min. Then, the temperature decreases again and becomes almost stationary at 243 K after 8 min of cooling. Again, supercooling can be observed in the experiments which is not accounted for in the numerical simulation. Apart from the supercooling effect, there is very good agreement between the experiment and numerical prediction. The deviation at the end of the solidification process is related to the fact that the non-homogeneous wall temperature conditions has a strong influence in this phase. Since the temperature distribution in the solid material of the chamber has not been integrated in the simulation, the deviation contributes to this deficiency as well.

Fig. 9 shows the temperature and velocity distributions as well as the liquid volume fraction at 120 s of freezing. As stated above, ice can be found on the walls

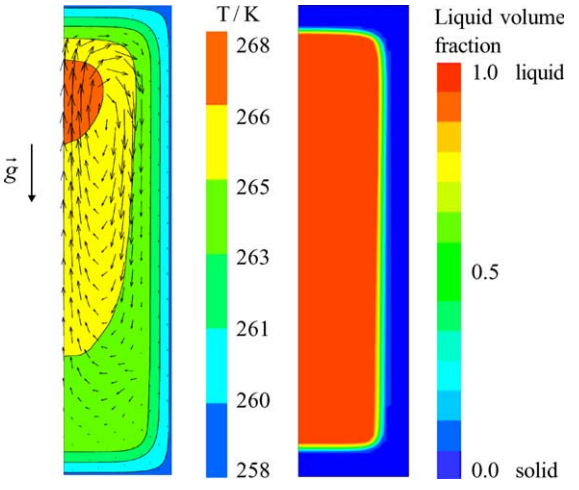

Fig. 9. The temperature and the liquid volume fraction distribution during freezing at 100 MPa.

while in the control point a temperature clearly above the solidification temperature can be observed. Only one vortex exists throughout the whole freezing process. In contrast to the case at atmospheric pressure the fluid motion occurs in clockwise direction. This implies a rather different mechanism of convective heat transfer under high hydrostatic pressure which is related to the vanishing density anomaly at elevated pressures. Furthermore, a slight irregularity in the ice front distribution can be observed. While on the top and on the vertical wall the thickness of the layers is almost constant, it is slightly larger on the bottom due to the effect of natural convection transporting warmer fluid upward and cooler fluid downward. The longest vectors in Fig. 9 correspond to velocity values of 0.5 mm s^{-1}.

4.3. HP-assisted freezing and thawing

Knowing that both convection and thermal time scales increase with the square of the typical chamber length scale we examine the interaction between fluid convection and formation of the ice front in a larger chamber. We consider HPAF/T in a hypothetic geometry, where the phase transition is governed by cooling/heating at elevated pressure. The compression is achieved by inflow of water into the chamber, leading to a dominating forced convection in this phase.

In this example the geometry of a HP-vessel is arbitrarily chosen and corresponds to that of a lab scale chamber, see Fig. 10. The diameter and the height of the chamber are chosen to be equal to $D = 30$ mm and the diameter of the inlet/outlet at the top is $d = 4$ mm. Thus the net volume amounts to 84 ml. It is assumed that the top and bottom walls are insulated and the temperature on the vertical walls can be controlled depending on the phases of the process. In this case an axis-symmetric 2D section is discretised with a mesh consisting of 150×75 grid points (spatial resolution of 0.2 mm).

At the beginning of the process the HP-chamber is filled with water at the temperature of 278 K and at atmospheric pressure. Due to inflow of an additional portion of water in the vessel, the pressure is increased. Water flows through an inlet/outlet section with a prescribed normal velocity of 1 mm s^{-1} during compression and of -5 mm s^{-1} (opposite direction) during decompression. The graphical presentation of the numerical results of the complete high pressure assisted freezing (HPAF) process in terms of the average temperature vs. pressure characteristics is demonstrated in Fig. 11.

An analysis of the average temperature gives only incomplete information about the process. No information about the formation of the ice-front and the termination of the phase transition can be obtained unless spatial and temporal distributions are accounted for. Therefore an analysis of the temperature distribution using numerical simulation completes very well the information about the process.

In the present case of HPAF/T, water is pressurised through 10 s up to 130 MPa ($A \rightarrow E$ in Fig. 11). Fig. 12 shows temperature distribution (left) and liquid volume fraction (right) after 10 s. It can be seen that the temperature of fluid in the chamber increases to about 280

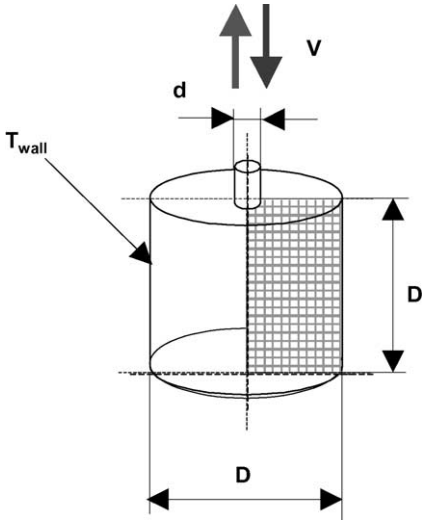

Fig. 10. Geometry of the HP-chamber.

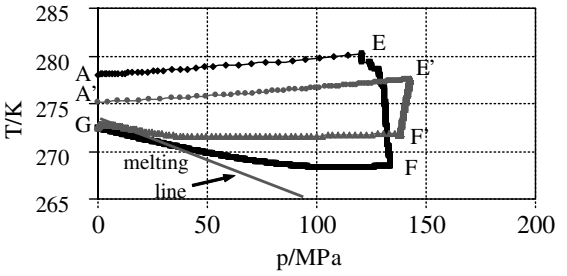

Fig. 11. Average temperature characteristics during the high pressure assisted freezing and thawing.

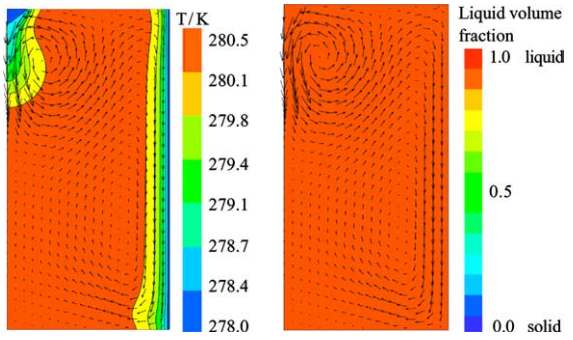

Fig. 12. HPAF at the end of the compression after 10 s.

K due to conversion of external work into internal energy. The inflowing water has a constant temperature of 278 K and mixes with the contained water due to forced convection. The pre-defined temperature of 278 K on the vertical wall creates buoyancy driven fluid motion near the walls. The liquid volume fraction is 100% at every location in the volume, indicating that no solidification takes place at this state of the process.

In the next phase the temperature on the vertical wall is decreased instantaneously to 258 K (E → F in Fig. 11). Since this temperature is below the melting temperature ice develops on the walls. The larger specific volume of ice 'I' with respect to water causes a pressure increase to 134 MPa. After 1 min of cooling, about 10% of the HP-chamber is occupied by the ice. The distributions of temperature and liquid volume fraction at the end of cooling are presented in Fig. 13. The fluid motion in the chamber is caused by buoyancy, which is more intensive compared to atmospheric conditions since the density dependency on the temperature is stronger at this pressure level. Heat transfer with the walls through the ice layer leads to a global decrease of the temperature. A temperature stratification can be observed which is disturbed by the convective motion close to the ice front. A temperature difference of approximately 18 K can be observed. The distribution of the liquid volume fraction shows the shape of the ice front. Close to the top wall, the ice layer is rather thin due to the comparably high water temperature at this location. At the bottom the layer exhibits a maximum thickness due to the low temperature at this location. From top to bottom, the layer increases in thickness irregularly which is a result of convective heat transfer along the ice layer. In the medium part, the flow is aligned on the ice front, leading to an intensive convective heat transfer, thus a continuous exhibition of the ice to warmer fluid coming from the top. Therefore, the ice growth rate is smaller at this location compared to the bottom. There, convective heat transfer is rather low due to a redirection of the flow field towards the centre. Consequently the ice layer is maximum and the growth rate is maximum as well.

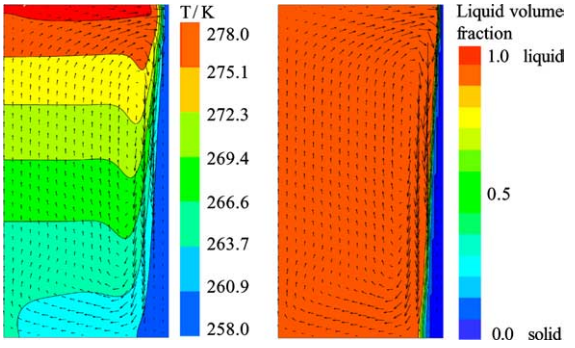

Fig. 13. HPAF at the end of cooling at 70 s (134 MPa).

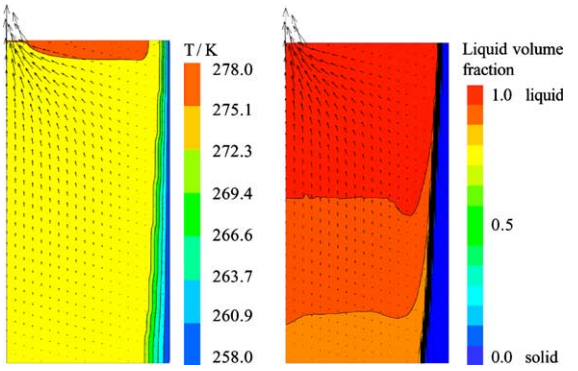

Fig. 14. HPAF at the end of the decompression at 72.3 s.

The volume fraction of ice increases to 14% when pressure is released (F → G in Fig. 11) by removing liquid from the chamber during 2.3 s. On this line the temperature rises because of release of latent heat. The temperature distribution and the liquid volume fraction at the end of decompression is presented in Fig. 14. Since the temperature distribution is almost homogeneous in the liquid volume and close to the phase limit, no further ice growth is observed in this part of the process. In turn, the temperature distribution allows a very fast freezing of a whole sample at atmospheric pressure by further cooling.

At this stage of the process one can recognize the importance of the knowledge about the involved time scales. In order to obtain a completely frozen state, the duration of the cooling has to be chosen in the appropriate way for each configuration (i.e. geometry, pressure medium, packaging material, food). Since the thermo-physical quantities and thus the time scales are pressure dependent, further knowledge about these parameters is required.

In order to observe pressure assisted thawing in the present configuration, the process is inverted. Newly inflowing water at 278 K leads to an increase of pressure to about 138 MPa (G → F′ in Fig. 11). Furthermore, a temperature of 278 K is applied instantaneously on the vertical wall. Fig. 15 shows the distribution of temperature and liquid volume fraction after a compression of approximately 12 s duration. As can be observed the layer of ice has thawed partially. The remaining solid region is detached from the wall. Strong free convection can be observed. The thawing of ice leads to a decrease of the temperature especially in the lower part of the chamber leading to the fact that the ice is melting from the top to the bottom.

Further application of the temperature 278 K on the wall during 300 s of the heating phase (F′ → E′ in Fig. 11) leads to a complete melting of the ice and a pressure increase up to 142 MPa. The obtained temperature surplus from the heating process allows the pressure

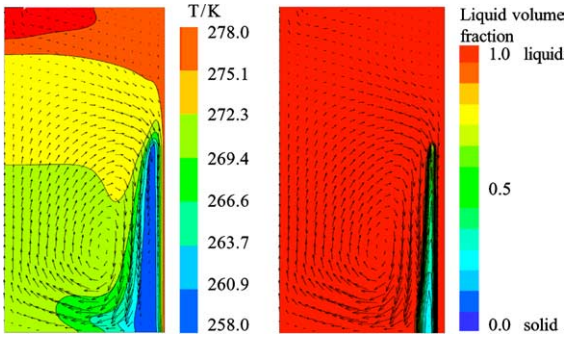

Fig. 15. HPAF—the end of G → F′-process.

release (E′ → A in Fig. 11) to atmospheric pressure without secondary ice formation. The choice of the correct parameters of the heating phase is very important since secondary crystallization during the subsequent decompression has to be avoided. In addition to the precedent discussion, it has to be stated, that the choice of the location of inflow/outflow orifices can be important for the control of the processes. Since ice formation during a cooling phase can block the orifice, a controlled decompression might be impossible as observed in a preceding analysis. In the current configuration, the orifice has been chosen to be in the centre of the top wall for this reason.

5. Conclusions and perspectives

High hydrostatic pressure induced freezing and thawing of water as a potential field of application of food technology is assessed by means of numerical simulation. Therefore, the enthalpy porosity method is enhanced accounting for phase changes of compressible media. The governing equations are derived in a continuum formulation following the ideas of Bennon and Incoprera [23] for this case. The numerical technique of linearisation in terms of the total enthalpy has been adapted to this case and successfully implemented in the CFX-4.4 code (ANSYS CFX). The comparison of numerical results to experimental results shows very good agreement for both atmospheric pressure and high hydrostatic pressure cases. It can be stated that the simulation requires a fine spatial resolution, a small time step and precisely described boundary conditions. Therefore, further optimisation of the computational model is needed.

It has been found, that convective fluid motion under high pressure has a different characteristics since the density anomaly of water disappears under high pressure. Thus, freezing/thawing processes, where free convection plays a major role, differ significantly from the atmospheric case when carried out under high hydrostatic pressure.

The shape of the ice formation is strongly influenced by convective transport of heat and momentum. For high pressure assisted freezing it can be observed, that the ice growth rate is reduced in regions where convective motion of the liquid fraction is intensive. Time scales of cooling/heating are highly important when complete freezing/thawing has to be achieved. Furthermore, since the shape of the ice front is irregular in convection driven ice formation, the position of inlet/outlet orifices has to be chosen with care in order to allow a control of pressure during decompression after (almost) complete freezing.

It is supposed that high pressure treatment and ice formation under high pressure can also influence migration of some ingredients within a food sample. However, these problems will remain subject of future investigations. Also the influence of a packing on the phase changes in liquid and solid systems will be investigated. Preliminary results show that packing has significant influence on the temperature distribution and, therefore, affects the time scales of the freezing and thawing.

Acknowledgements

This work is supported by "Bundesministerium für Bildung und Forschung" (German Ministry of Education and Science), within the project No. 0330098. We gratefully acknowledge the Institute of Food Biotechnology and Food Process Engineering, Technical University of Berlin for their supply of experimental results.

References

[1] F. Harte, M. Amonte, L. Luedecke, B.G. Swanson, G.V. Barbosa-Canovas, Yield stress and microstructure of set yogurt made from high hydrostatic pressure-treated full fat milk, J. Food Sci. 67 (2002) 2245–2250.
[2] B. Krebbers, A.M. Matser, M. Koets, R.W. Van den Berg, Quality and storage-stability of high-pressure preserved green beans, J. Food Eng. 54 (2002) 27–33.
[3] P. Butz, R. Edenharder, A.F. Garcia, H. Fister, C. Merkel, B. Tauscher, Changes in functional properties of vegetables induced by high pressure treatment, Food Res. Int. 35 (2002) 295–300.
[4] D. Fachin, A. van Loey, A. Indrawati, L. Ludikhuyze, M. Hendrickx, Thermal and high-pressure inactivation of tomato polygalacturonase: a kinetic study, J. Food Sci. 67 (2002) 1610–1615.
[5] J.C. Cheftel, M. Thiebaud, E. Dumay, Pressure-assisted freezing and thawing of foods: a review of recent studies, High Pressure Res. 22 (2002) 601–611.
[6] M.T. Kalichevsky, D. Knorr, P.J. Lillford, Potential food applications of high-pressure effects on ice–water transitions, Trends Food Sci. Technol. 6 (1995) 253–259.

[7] A. LeBail, D. Chevalier, D.M. Mussa, M. Ghoul, High pressure freezing and thawing of foods: a review, Int. J. Refrig. 25 (2002) 504–513.
[8] A. Saul, W. Wagner, A fundamental equation for water covering in the range from the melting line to 1273 K at pressures up to 25000 MPa, J. Phys. Chem. Ref. Data 18 (1989) 1537–1564.
[9] O.V. Nagornov, V.E. Chizhov, Thermodynamic properties of ice, water and a mixture of the two at high pressure, J. Appl. Mech. Tech. Phys. 31 (1990) 378–385.
[10] P. Först, F. Werner, A. Delgado, The viscosity of water—especially at subzero degrees centigrade, Rheol. Acta 39 (2000) 566–573.
[11] M. Pehl, A. Delgado, An in situ technique to visualize temperature and velocity fields in liquid biotechnical substances at high pressure, in: H. Ludwig (Ed.), Advances in High Pressure Bioscience and Biotechnology, Springer, Heidelberg, 1999, pp. 519–522.
[12] M. Pehl, F. Werner, A. Delgado, First visualization of temperature fields in liquids at high pressure, Exp. Fluids 29 (2000) 302–304.
[13] C. Hartmann, Numerical simulation of thermodynamic and fluid-dynamic processes during the high-pressure treatment of liquid food systems, Innovative Food Sci. Emerg. Technol. 3 (2002) 11–18.
[14] C. Hartmann, A. Delgado, Numerical simulation of convective and diffusive transport effects on a high-pressure-induced inactivation process, Biotechnol. Bioeng. 79 (1) (2002) 94–104.
[15] C. Hartmann, A. Delgado, J. Szymczyk, Convective and diffusive transport effects in a high pressure induced inactivation process of packed food, J. Food Eng. 59 (2003) 33–44.
[16] S. Denys, A.M. Van Loey, M.E. Hendrickx, Modeling conductive heat transfer during high pressure thawing processes: determination of latent heat as a function of pressure, Biotechnol. Progr. 16 (2000) 447–455.
[17] P.D. Sanz, L. Otero, High pressure shift freezing. Part 2. Modeling of freezing times for a finite sylindrical model, Biotechnol. Progr. 16 (2000) 1037–1043.
[18] J.M. Chourot, R. Lemaire, G. Cornier, A. Le Bail, Modeling of high pressure thawing, in: R. Hayashi (Ed.), High Pressure Bioscience and Biotechnology, 1996, pp. 439–444.
[19] M. Giangi, T.A. Kowalewski, F. Stella, E. Leonardi, Natural convection during ice formation: numerical simulation vs. experimental results, Comput. Assisted Mech. Eng. Sci. 7 (2000) 321–342.
[20] J. Ni, F.P. Incropera, Extension of the continuum model for transport phenomena occuring during metal alloy solidification-I. The conservation equations, Int. J. Heat Mass Transfer 38 (7) (1995) 1271–1284.
[21] A.D. Brend, V.R. Voller, K.J. Reid, Enthalpy–porosity technique for modelling convection–diffusion phase change: application to the melting of a pure metal, Numer. Heat Transfer 13 (1988) 297–318.
[22] V.R. Voller, C. Prakash, A fixed grid numerical modelling methodology for convection–diffusion mushy region phase-change problems, Int. J. Heat Mass Transfer 30 (8) (1987) 1709–1719.
[23] W.D. Bennon, F.P. Incropera, A continuum model for momentum, heat and species transport in binary solid-liquid phase change systems—I. Model formulation, Int. J. Heat Mass Transfer 30 (10) (1987) 2161–2170.
[24] V.R. Voller, A.D. Brent, C. Prakasch, The modelling of heat, mass and solute transport in solidification systems, Int. J. Heat Mass Transfer 32 (9) (1989) 1719–1731.
[25] J. Banaszek, Y. Jaluria, T.A. Kowalewski, M. Rebow, Semi-implicit FEM analysis of natural convection in freezing water, Numer. Heat Transfer, Part A 36 (1999) 449–472.